# Journal of Materials Chemistry C

Accepted Manuscript


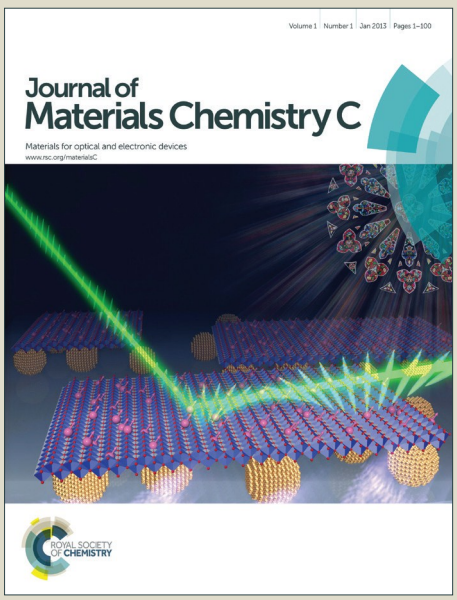





ROYAL SOCIETY OF CHEMISTRY

www.rsc.org/materialsC

Journal Name

ARTICLE TYPE

Cite this: DOI: 10.1039/xxxxxxxxxx

# Stability and electronic properties of new inorganic perovskites from high-throughput ab initio calculations†

Sabine Körbel,[a,b‡] Miguel A.L. Marques,[c,d] and Silvana Botti*[a,d]

Received Date
Accepted Date

DOI: 10.1039/xxxxxxxxxx

www.rsc.org/journalname

Using a high-throughput approach based on density functional theory, we perform an extensive study of possible $ABX_3$ perovskites, where $X$ is a non-metal and $A$ and $B$ span a large portion of the periodic table. We calculate the ternary phase diagram for each composition and we discuss the thermodynamic stability of perovskite phases. We find a large number of $ABX_3$ perovskites, which are still absent from available databases, and which are stable with respect to decomposition into known ternary, binary or elementary phases. For these structures, we then calculate electronic band gaps, hole effective masses, and the spontaneous ferroelectric and magnetic polarization, which are relevant material properties for a number of specific applications in photovoltaics, transparent contacts, piezoelectrics, and magnetoelectrics. Some of our novel perovskites exhibit promising properties for applications.

## 1 Introduction

It is a well-known fact that the compounds belonging to the family of perovskites show a remarkable variety and interplay of mechanical, electric, magnetic, optical, and transport properties.[1–5] An ideal perovskite with the general formula $ABX_3$ consists of corner sharing octahedra of $X$ anions with $B$ cations in their center, and $A$ cations occupying the 12-fold coordinated site located in the middle of the cube constituted by eight octahedra. Its crystal structure is the simple cubic structure of $CaTiO_3$ (see Fig. 1). However, the ideal cubic structure is rather uncommon, and many distorted variants are observed in natural and synthetically fabricated minerals. The reason for the large range of possible compositions and material properties resides in the fact that the perovskite crystal structure is able to accommodate atoms $A$, $B$, and $X$ of different sizes and with different oxidation states. Perovskites are nowadays key materials for many technologies essential to our modern society. A few examples include piezoelectrics,[1,2] high-$k$ dielectrics,[1,2] photovoltaic absorbers,[3] and multiferroic magnetoelectrics.[4]

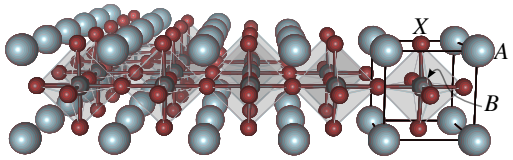


**Fig. 1** (Color online) The perovskite structure with the 12-fold coordinated $A$ cations (light blue) and the octahedrally coordinated $B$ cations (gray). The $X$ anions (red) are located at the vertices of corner sharing octahedra. The five-atom unit cell is indicated by black lines.

Although many perovskites are already known experimentally, considering the vast number of possible combinations of three chemical elements, the family of perovskites could be considerably larger and possibly interesting systems are still awaiting our discovery. The main objective of this paper is therefore to provide a list of $ABX_3$ compositions where the perovskite structure (allowing for small distortions) is thermodynamically stable with respect to decomposition in already known ternary, binary and elementary compounds.

Our main motivation comes from two important technological areas where perovskites are key materials: piezoelectrics and photovoltaics. In the first case, $Pb(Ti,Zr)O_3$ has excellent piezoelectric properties and has been used in piezoelectric actuators for many years. In the second, lead-based "hybrid" organic-inorganic perovskites, such as $CH_3NH_3PbI_3$ ($MAPbI_3$)[3], turn out to be extraordinarily efficient photovoltaic absorbers, for which higher and higher energy conversion efficiency records are being re-

[a] Institut für Festkörpertheorie und -optik, Friedrich-Schiller-Universität Jena, Max-Wien-Platz 1, 07743 Jena, Germany
[b] Institut Lumière Matière, UMR5306 Université Lyon 1-CNRS, Université de Lyon, F-69622 Villeurbanne Cedex, France
[c] Institut für Physik, Martin-Luther-Universität Halle-Wittenberg, D-06099 Halle, Germany
[d] European Theoretical Spectroscopy Facility
* E-mail: silvana.botti@uni-jena.de
‡ E-mail: skoerbel@uni-muenster.de
† Electronic Supplementary Information (ESI) available: Tables with all calculation results. See DOI: 10.1039/b000000x/

ported.[6,7] Furthermore, this extraordinary rise up to an efficiency of 20% has happened in a mere six years, clearly proving the enormous potential of perovskites for this specific application. Beside the high absorption coefficient, the superior absorption properties of $MAPbI3_3$ have also been ascribed to small effective masses of electrons and holes,[8] and also to the benign nature of defects.[9]

These lead-based materials have excellent properties and contain elements that are both cheap and abundant. However, the presence of lead leads to several problems due to its toxicity, and alternative materials are being actively sought. In the case of photovoltaic absorbers, lead-based perovskites possess another considerable disadvantage that impedes their industrial implementation: They tend to partially decompose when exposed to air, water, ultra-violet light, or heat.[10,11] Several substitutions have been attempted to replace lead: $(K,Na)NbO_3$ and $(Bi,Na)TiO_3$ are possible candidates for piezoelectric devices, but so far the performance of $Pb(Ti,Zr)O_3$ remains superior. Lead in $CH_3NH_3PbI_3$ has been successfully replaced by Sn, however, stability issues worsen.[6,12] Recently, it has been proposed, based on ab *initio calculations*, to replace Pb by Tl and Bi,[13] which may improve the stability of the perovskite, but would not solve the problem of toxicity, or by In and Bi, which are less toxic but yield less stable structures.[13] Alternatively, it has been proposed to replace $(MA)^+Pb^{2+}I_3^-$ by a compound of the form $(OC)^{2+}(IV)^{4+}C_3^{2-}$, such as $NH_3NH_3ZrS_3$, where OC is a divalent organic cation, IV is a tetravalent metal, and $C$ is a chalcogen.[14] Such compounds may be thermodynamically more stable than $MAPbI_3$, however it has still to be proven whether the extraordinary performance as absorber and charge conductor of $MAPbI_3$ can be retained.

In this context, the search of new perovskites is a critical step for the further development of these technologies on a large scale. The problem of finding new materials for specific applications has recently gained momentum thanks to the possibility of screening large sets of materials by performing *ab initio* calculations. Using efficient and accurate numerical methods for electronic structure calculations, such as density-functional theory (DFT), promising compounds can be identified and proposed for synthesis. This approach has already been successfully applied, e.g., to battery materials[15], super-hard materials[16], transparent conducting oxides,[17,18] organic polymer dielectrics,[19] and hard magnets,[20] to name just a few examples.

In this work we present high-throughput calculations of perovskites, focusing on their photovoltaic, piezoelectric and magnetic properties. The targets of our search are thermodynamically stable compounds which are possibly non-toxic, made of abundant elements, easy to produce and at least as efficient as the lead-based perovskites. Thermodynamic stability is desirable for at least three reasons: A stable compound is, in general, easier to synthesize, tends to be more resistant against damage by, e.g., radiation or heat, and can act as a stabilizer in a solid solution of two perovskites.

To this purpose, we perform in this Article a systematic search of all possible thermodynamically stable perovskites of the type $ABX_3$, where $X$ is N, O, F, S, Cl, Se, Br, Te, or I, and $A$ and $B$ can be all elements up to Bi, excluding rare gases and lanthanides. We do not impose strictly the symmetry of the cubic perovskite phase, but allow for distortions of the five atom unit cell. We also consider other recurring crystal structures with the same stoichiometry but with more atoms per unit cell, and check if they are more stable than the distorted perovskite structure. We then characterize the materials that are thermodynamically stable by calculating a series of properties, namely the electronic band-gap, the hole effective mass, and the spontaneous ferroelectric and magnetic polarization.

Of course, this is not the first high-throughput investigation of perovskites, and in fact several studies have appeared in the literature in recent years. However, these studies consider either a relatively small set of stoichiometries or a very small set of properties. Furthermore, the important problem of thermodynamic stability is hardly ever addressed. For example, Caracas and Cohen[21] investigated oxynitride perovskites, with the chemical formula $ABO_2N$, with $A$=Y, In, Ga, or Bi, and $B$=Si, Ge, Ti, Zr, C, or Sn. Armiento *et al.*[22] performed a large-scale screening of oxide perovskites of the form $ABO_3$, in order to find suitable "binary" compounds of the form $ABO_3 - A'B'O_3$ which are likely to exhibit a morphotropic phase boundary, a composition at which two different crystal structures are close in energy and the ferroelectric polarization can be easily rotated, giving rise to high piezoelectric responses. Perovskites of the form $ABX_3$, with $X$=O, N, S, F, and combinations thereof, were studied by Castelli *et al.*[23,24] with water splitting as the target application. Filip *et al.*[25] calculated band gaps of about 20 metal halide perovskites, concentrating on the effect of octahedral tilting on the size of the band gap. Finally, Brehm *et al.*[26] investigated sulfides with nine different elements on $A$ sites and six transition metals on $B$ sites.

The remaining of this Article is structured as follows: In sections 2 and 3 we describe our methodology and give numerical details on the calculations. Section 4 contains a discussion of thermodynamic stability, ground-state structures, band gaps and ferroelectric polarization. The paper closes with a conclusion and outlook in section 5. Tables with all the calculated properties are provided as Electronic Supplementary Information (ESI†).

## 2 Methods

The search space that we are addressing contains more than 32 000 compounds. In order to make our calculations feasible we have to follow a strategy by steps.

(i) We start by building all possible $ABX_3$ compounds, where $X$ is N, O, F, S, Cl, Se, Br, Te, or I, and $A$ and $B$ can be all elements up to Bi, excluding rare gases and lanthanides, see Fig. 2. We impose a cubic perovskite structure (space group #221, $Pm\bar{3}m$) with five atoms in the unit cell. We then optimize the lattice constant. This first screening step can be performed very efficiently due to the high symmetry of the cubic structure.

(ii) The next step is the calculation of the distance of the cubic $ABX_3$ phase to the convex hull of thermodynamic stability. We recall that the convex hull is a hypersurface in composition space that connects all compounds that are thermodynamically stable, i.e., that have an energy lower than all possible decomposition channels (for more details, see also the ESI†).

Our theoretical convex hull contains all stable reservoir compounds present in the Materials Project database[28] and the Open

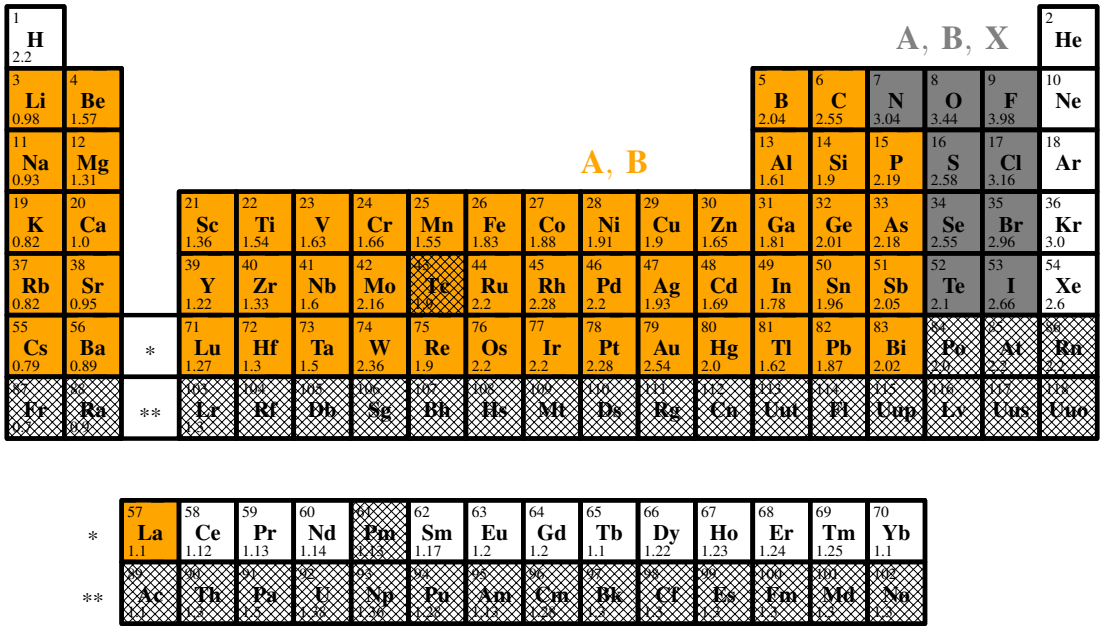


**Fig. 2** (Color online) Periodic system of the elements considered in the $ABX_3$ compounds, with $X$ anions shaded in grey. All shaded elements, including those shaded in grey, were considered for $A$ and $B$ sites. Radioactive elements are hatched. The number in the left lower corner of each element field is its Pauling electronegativity.[27]

Quantum Materials Database.[29] Note that our calculations are performed at zero temperature and pressure for perfect periodic crystals.

(iii) At this point we remove from our dataset all compositions that are highly unstable, i.e., that appear more than 100 meV/atom above the convex hull of stability. We emphasize that this does not mean that the composition is unstable, as it could adopt another crystal structure in order to decrease its energy. However, we are here interested in finding perovskite structures, and it is unlikely that a small distortion of the cubic perovskite can decrease the energy by more than 100 meV/atom. We also conserve those compositions that are expected to have more chances to be stable perovskites according to empirical rules (ionic charge neutrality and Goldschmidt tolerance factors between 0.75 and 1.25)[30], even if their distance to the convex hull is larger than 100 meV/atom. Ionic radii to calculate Goldschmidt tolerance factors are taken from Ref. 31. This first selection reduces the number of candidate structures to $\approx 5000$.

(iv) Very often, the ground state structure of a perovskite compound lowers its energy by slightly distorting from the ideal cubic one. Such a distortion occurs in, e.g., $PbTiO_3$, $BaTiO_3$, $KNbO_3$, and in many other perovskites. In order to allow for such distortions, we therefore break all symmetries by creating a frozen optical phonon at Γ, before performing a second geometry optimization of the compounds that have passed stage (iii). On the other hand, removing the symmetries allows the compounds to adopt crystal structures other than the ideal or distorted perovskite. Note that at this stage we still have five atoms in the unit cell, therefore deformations due to imaginary phonons outside Γ are not accessible. Another typical distortion in perovskites that can lower the energy is a rotation of the octahedra about one or more of their axes. Octahedral rotations are not accessible within our 5-atom unit cell, so in order to not miss structures that are stabilized by octahedral rotations, we calculate the energy of a perovskite prototype with octahedral rotation [the ground state of $NaNbO_3$, space group no. 161 ($R3c$)]. If a compound is stable in this structure, it remains on our list. It is true that other possible octahedral rotation modes might further stabilize the compound, but apparently different rotation modes have similar energies: out of 24 tested cases, for 13 the energy difference between different octahedral rotation modes was below about 20 meV/atom, and in the remaining cases the energy differences between paraelectric and ferroelectric case were large, above 50 meV/atom, so that the larger energy differences between different rotational modes may be ascribed to ferroelectric or antiferroelectric displacements that accompany the rotational modes, rather than to the rotational modes themselves.

In the following, we keep speaking of a "perovskite" even if the structure is to some extent distorted from the ideal cubic one. More precisely, we allow for distortions up to 20% in the cell parameters, and up to 10° in the cell angles with respect to the ideal cubic perovskite structure. For comparison: $PbTiO_3$ has a distortion in the lattice parameters by about 6% (a tetragonal $c/a$ ratio of about 1.06).[32]

(v) It is well known that unstable phases can be stabilized by temperature, pressure, defects, dopants, or growth on an appropriate substrate. Moreover, due to the theoretical error associated to the calculation of the total energy, an inversion of the ordering of the phases very close in energy is always possible. In view of the above, we believe it is always relevant to discuss all compositions that are either thermodynamically stable or quasi-stable [within a threshold that we fix equal to 25 meV (room tempera-

ture) from the convex hull]. Of the resulting compounds, those which have remained perovskites and are at most 25 meV/atom above the convex hull are further tested for stability by comparing their formation energies to those of a set of prototype crystal structures. The selected prototypes are common $ABX_3$ crystal structures which are not perovskites. Except for potassium chlorate and salpeter, the prototypes have in common with perovskites the presence of a network of $BX_6$ octahedra. However, the octahedra can be connected in different ways: by corner-sharing as in perovskites, or edge- or face-sharing, or a combination. In this way, our selection of prototypes is representative for the different structural motifs that can be found in $ABX_3$ compounds. The prototypes we selected are listed in Table 1. If we find a prototype structure that is lower in energy than the perovskite structure by more than 25 meV, the corresponding composition is discarded. This step reduces the size of our set of perovskites to 199 compounds.

**Table 1** Prototype crystal structures of $ABX_3$ compounds included in the convex hull, space group (SG) number and symbol, number of atoms (sites) in the unit cell $n_{\text{sites}}$, and connection of neighboring octahedra (corner-sharing CS as in perovskites, or edge-sharing ES, or face-sharing FS)

| prototype | SG | $n_{\text{sites}}$ | octahedra |
|---|---|---|---|
| potassium chlorate | 11 ($P2_1/m$) | 10 | – |
| pyroxene | 15 ($C2/c$) | 20 | ES |
| $NH_4CdCl_3$ ($CsPbI_3$) | 62 ($Pnma$) | 20 | ES |
| $CaIrO_3$ | 63 ($Cmcm$) | 10 | ES, CS |
| ilmenite | 148 ($R\bar{3}$) | 10 | FS, ES |
| salpeter | 160 ($R3m$) | 5 | – |
| pyrochlore | 227 ($Fd\bar{3}m$) | 20 | CS |

(vi) The final set of perovskites contains 128 compounds that are already contained in experimental databases, while 71 compounds are new. We then characterize these perovskites by calculating a variety of electronic properties, namely the electronic band-gap, the average hole effective mass, the magnetic moment, and the spontaneous electric polarization. This latter property is estimated using the Born effective charges as

$$\mathbf{P} = \sum_i \underline{\underline{Z}}^*_i \mathbf{u}_i, \tag{1}$$

where $\underline{\underline{Z}}^*_i$ is the Born-effective charge tensor of atom $i$, and $\mathbf{u}_i$ is the displacement of atom $i$ from the inversion-symmetric site it would occupy in the ideal cubic perovskite structure. This ferroelectric polarization is only meaningful if the DFT band gap is larger than zero, since a metal cannot have a spontaneous electric polarization.

At this stage, for the perovskites that exhibit a sizeable ferroelectric polarization in the five-atom unit cell ($> 10\ \mu$C/cm$^2$), we test their thermodynamic stability with respect to an antiferroelectric perovskite structure with an octahedral rotation [$PbZrO_3$, space group no. 55 ($Pcma$), 40 atoms in the unit cell], and a paraelectric perovskite crystal structure also with an octahedral rotation [$SrTiO_3$, space group no. 140 ($I4/mcm$), 10 atoms in the unit cell]. It is important to include such prototypes since antiferroelectric and rotational distortions of the octrahedra network are inaccessible using five-atom unit cells. However, they can compete with and win over the ferroelectric distorsion. As an example, if a five-atom unit cell is assumed for $PbZrO_3$, a fairly large ferroelectric polarization of 71 $\mu$C/cm$^2$ is obtained, whereas the true ground state is antiferroelectric with octahedral rotations.

## 3 Computational Details

Except when stated otherwise, calculations are performed with DFT in the generalized-gradient approximation of Perdew, Burke and Ernzerhof[33] (PBE) for the exchange-correlation functional, using VASP, the Vienna Ab initio Simulation Package[34]. We use the projector-augmented wave (PAW) method, a basis of plane waves with energies up to 520 eV, and Γ-centered Monkhorst-Pack $k$-point meshes with an approximately constant $k$-point density of about 500 $k$-points per Å$^{-3}$, which corresponds to $k$ meshes including $10\times10\times10$ $k$ points for a simple cubic cell with a lattice parameter of 5 Å. Our calculations include spin-polarization. In cases where we find a ferromagnetic ground state, its formation energy is compared to those of two antiferromagnetic configurations, and the final magnetic moment is taken from the lowest-energy state of the three. The two antiferromagnetic states are obtained by doubling the optimized perovskite unit cell along the pseudocubic $\langle001\rangle$ and the $\langle111\rangle$ directions (in-plane and rocksalt-like fcc configuration of equal spins). The magnetic properties of the interesting candidate perovskites should however be further studied with more sophisticated methods, such as DFT with a Hubbard parameter (DFT+$U$) to obtain reliable predictions of the ground-state spin configuration. Unfortunately, the Hubbard $U$ is not entirely unique and transferable but should be carefully adapted to the compound and property of interest. As this unsystematic procedure is unsuited for high-throughput studies, we decided not to use DFT+$U$ in this work. The PAW setups are taken from version 5.3 of VASP. The convex hull is obtained based on the "quickhull" algorithm of Barber and coworkers[35] using the reservoir compounds present in the Materials Project[28] Database and in the Open Quantum Materials Database.[29] Entropic effects are neglected, as they are expected to play only a minor role for these systems.

Due to the well-know band-gap problem in standard DFT, we use the hybrid exchange-correlation functional of Heyd, Scuseria, and Ernzerhof (HSE06)[36] to calculate band structures. As the HSE functional makes the calculations computationally more demanding, we reduce the $k$-point density to about 60 $k$-points per Å$^{-3}$, which corresponds to meshes including $5\times5\times5$ $k$-points for the simple cubic cell with edge length 5Å. Note that the band gaps are calculated for structures with five atoms per unit cell, some of them containing an odd number of electrons.

Effective masses are calculated within the program BoltzTraP[37], assuming ambient temperature (300 K) and a doping level of $10^{18}$/cm$^3$. Effective mass tensors $\underline{\underline{M}}$ are then calculated as

$$\langle\left(M^{-1}\right)_{\alpha\beta}\rangle = \frac{\sum_n \int \mathrm{d}\mathbf{k} \frac{\partial^2 \varepsilon_{n\mathbf{k}}}{\partial k_\alpha \partial k_\beta} f_{n\mathbf{k}}}{\sum_n \int \mathrm{d}\mathbf{k} f_{n\mathbf{k}}}, \tag{2}$$

where $n$ is the band index, the energy eigenvalues $\varepsilon_{n\mathbf{k}}$ are taken from a Fourier-interpolated band structure, and $f_{n\mathbf{k}}$ is the Fermi distribution. The latter depends on the chemical potential $\mu$,

which is adjusted by the doping level. The inverse mass tensors are afterwards inverted, and their eigenvalues are averaged over the three directions. In this way, our method is identical to that of Hautier *at al.*[18], with the exception that we interpolate the band structure in the whole Brillouin zone, but starting from the grid of our ground state calculations, whereas in Ref. 18, a fine band structure along several high-symmetry lines was used for averaging the effective masses over the Brillouin zone. With this approach, we may not detect all candidates with high carrier mobility, because our single-band model for the effective mass does not account for good mobility due to degenerate bands.

Finally, Born effective charges are obtained with a combination of perturbation theory and finite differences as explained in Ref. 38. We observed that the calculated spontaneous electric polarization is a sensitive function of the cell volume and exchange-correlation functional. We compared results from PBE and the local-density approximation (LDA) for $KNbO_3$, $BaTiO_3$, and $PbTiO_3$, and found that with the PBE functional, ferroelectric polarization and/or strain are overestimated for $BaTiO_3$ and $PbTiO_3$, whereas the LDA yields good agreement with experiment. In the case of $KNbO_3$, the experimental data have some spread, and the two functionals yield comparable agreement with experiment. As an example, for $PbTiO_3$ we obtain a ferroelectric polarization of 119 $\mu$C/cm$^2$, much larger than the experimental value of 75 $\mu$C/cm$^2$,[39] while the LDA yields the excellent result of 73 $\mu$C/cm$^2$. Whereas with PBE we obtain a tetragonal $c/a$ ratio of $c/a$=1.21, with the LDA we obtain $c/a$=1.04, much closer to the experimental value of $c/a$=1.06.[32] We have therefore decided to use the LDA to calculate the spontaneous polarization.

## 4 Results and Discussion

In this section we give a summary of the material properties for all the 199 compounds belonging to our final set of perovskites, 71 of which are not yet listed in materials databases. The complete results can be found in Tables ESI-1 to ESI-4 of the ESI.[†]

Altogether, there are 21 $ABX_3$ perovskites in the MP, OQMD, and Demo version of ICSD databases which we do not detect. Of those, 11 ($KCrF_3$, $BaIrO_3$, $LuCoO_3$, $SrOsO_3$, $BaOsO_3$, $KTeO_3$, $NiPtO_3$, $KOsO_3$, $MgSiO_3$, and $ScAlO_3$) are more than 25 meV/atom above the convex hull at zero pressure in all the structures that we tested. Two ($CaMoO_3$ and $BaFeO_3$) are more than 100 meV/atom above the hull in the cubic perovskite structure and were therefore discarded. One ($BaCoO_3$) is a layered non-perovskite structure with face-sharing octahedra in the ground state. The remaining seven ($NaMgF_3$, $CaRuO_3$, $CaIrO_3$, $TlNbO_3$, $TlTaO_3$, $LiTcO_3$, and $CsNbO_3$) are considerably distorted perovskites that are not detected with the structural criteria that we use to numerically distinguish a perovskite from a non-perovskite.

### 4.1 Chemical composition of stable perovskites

We will start by looking at the problem of the stability of the perovskite structure by itself. As we have data for a very large number of compositions, we can perform a simple statistical analysis. Figure 3 shows the frequency of occurrence of the chemical elements on the $A$, $B$, and $X$ sites of the $ABX_3$ structure. The $A$ site is most often occupied by a large alkali or alkali-earth metal. Also a few mono- and divalent metals such as Pb, Ag, etc. can occupy that position. Perhaps a bit surprising is the large value for the occurrence of Tl. This can be understood by the striking chemical similarity between Tl and the large alkali metals,[40] but it is also possible that the stability of these perovskites is overestimated as the binary phases of Tl are certainly much less studied than the ones including its neighbors.

The $B$ site accommodates many more elements. The most likely ones are, surprisingly, Ge and Ca, but the distribution is very broad. Note that some elements, like Ag, Pb, or In, can actually occupy either the $A$ or $B$ position, depending on the second cation. Finally, we see that the probability of finding a non-metal in the $X$ position of stable perovskites increases essentially with the electronegativity of the element, while the size of the non-metal seems to play a smaller role. $BaHfS_3$, $BaZrS_3$, and $BaZrSe_3$ are the only chalcogenide perovskites that we find stable, in line with the recent observation of Brehm *et al.*[26] that chalcogenides, other than oxides, are unstable in the perovskite structure with corner-sharing octahedra, and instead prefer crystal structures with edge-sharing octahedra. There is no stable telluride perovskite. Similarly, we only find three stable nitride perovskites, $LaReN_3$ and $YReN_3$ (both metals) and $LaWN_3$ (a semiconductor).[41] We will discuss the properties of $LaWN_3$ in detail below. Finally, we note that a few known perovskites, such as $YReN_3$,[41] do not appear automatically in our list of stable perovskites. The reason is that these compounds crystallize in a distorted perovskite structure with a unit cell larger than the five-atom cells we have studied here, and in some cases, the structural rearrangement enabled in this larger unit cell can lead to a gain in free energy larger than our stability threshold of 25 meV/atom. This effect is particularly strong in the case of $YReN_3$, which we recently found to be stable in a perovskite structure with a larger unit cell with an octahedral rotation.[41] This octahedral rotation decreases the total energy by 137 meV/atom. This observation leads us to conclude that more perovskites can be likely stabilized using larger protype structures with 10, 15, 20, or more atoms per unit cell.

We find several Cs metal halides, including $CsPbI_3$. However, in agreement with experiment[42], we find that $CsPbI_3$ has a non-perovskite ground state with edge-sharing octahedra; the perovskite structure is therefore metastable.

### 4.2 Band gaps

Figure 4 shows the band gap of the perovskites with a band gap larger than 0.5 eV contained in our final set, ordered by the value of the indirect gap. These band gaps were obtained using the hybrid HSE06 exchange-correlation functional. The band gap region most interesting for photovoltaic absorbers is shaded in blue. Here we include also compounds with slightly too small or slightly too large band gaps for the following reasons: (a) in our five-atom unit cells, we cannot access all possible structural instabilities, like octahedral rotations, which may lower the formation energy of the compound and open the gap, (b) we have neglected spin-orbit coupling, which may decrease the band gaps

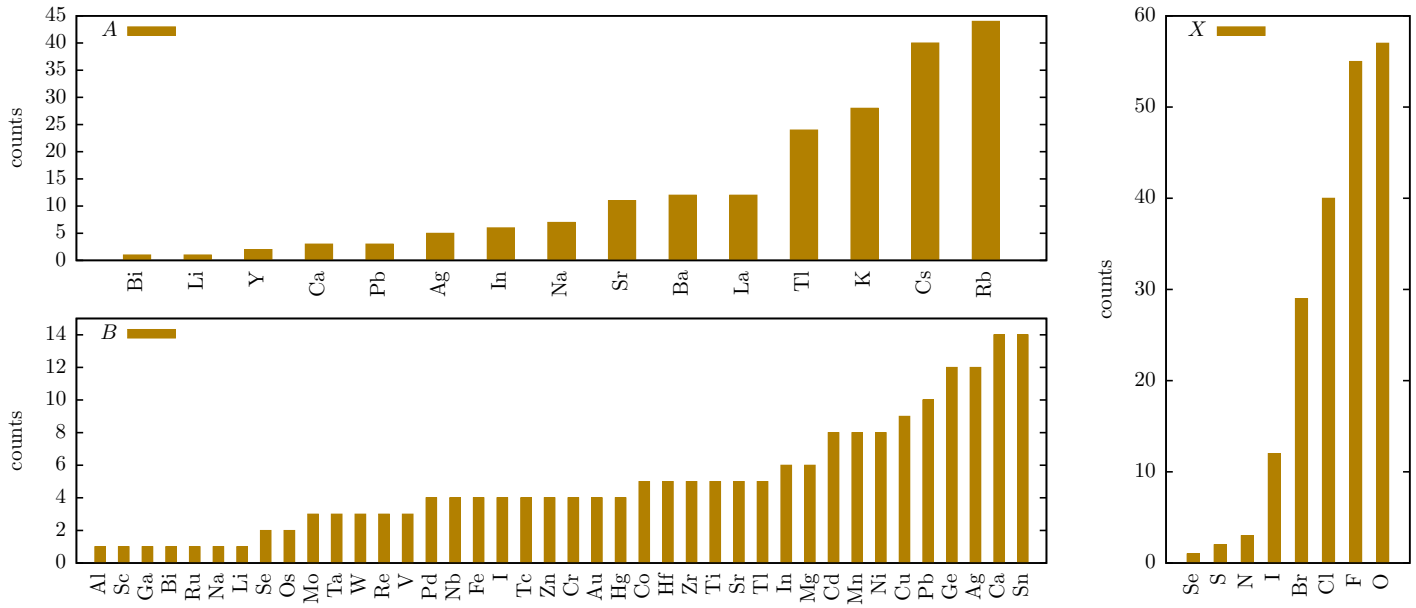


**Fig. 3** (Color online) Frequency of occurrence of the elements in the final set of perovskite compounds.

**Table 2** Calculated HSE band gaps, spontaneous electric polarization $|P|$, effective hole mass $m_h^*$, and distance from the convex hull of stability $E_{\text{hull}}$ in eV/atom of $ABX_3$ perovskites with gaps interesting for photovoltaics. New compounds are marked by a •

| composition | HSE gap ind. | HSE gap direct | $\|P\|$ ($\mu$C/cm$^2$) | $m_h^*$ | $E_{\text{hull}}$ |
|---|---|---|---|---|---|
| $CsSnCl_3$ | 1.57 | 1.57 | 1 | 0.14 | 0.000 |
| $CsGeI_3$ | 1.48 | 1.48 | 7 | 0.29 | 0.000 |
| $CsSnBr_3$ | 1.11 | 1.11 | 1 | 0.11 | 0.000 |
| $RbGeBr_3$ | 1.65 | 1.65 | 4 | 0.25 | 0.004 |
| $RbSnBr_3$• | 1.10 | 1.10 | 3 | 0.19 | 0.005 |
| $BaPbO_3$ | 0.64 | 1.35 | 0 | 0.00 | 0.007 |
| $CsSnI_3$ | 0.85 | 0.85 | 4 | 0.12 | 0.009 |
| $InSnBr_3$ | 1.58 | 1.58 | 0 | 0.25 | 0.011 |
| $RbGeI_3$ | 1.35 | 1.35 | 8 | 0.31 | 0.020 |
| $RbSnCl_3$• | 1.61 | 1.61 | 3 | 0.22 | 0.022 |
| $KGeBr_3$• | 1.47 | 1.47 | 7 | 0.22 | 0.026 |
| $RbSnI_3$ | 0.82 | 0.82 | 3 | 0.11 | 0.036 |
| $TlGeBr_3$• | 1.28 | 1.28 | 0 | 0.21 | 0.040 |
| $BaZrSe_3$• | 1.01 | 1.44 | 0 | 0.82 | 0.072 |

of some of the compounds, as we discuss further below. (c) the band gap calculated with HSE06 can still differ by 10-20% with respect to the experimental band gap. In the case of $BaSnO_3$, the band gap varies particularly strongly with the volume of the unit cell[43]. Because of a small volume overestimation, which is typical for the PBE functional, in the HSE calculation at the PBE volume we obtain a band gap that is considerably smaller than the experimental one (Experiment: ≈3.1 eV[44]; calculation: 2.34 eV).

Several compounds have an indirect band gap in this range (see Table 2), and a few of these are direct (or quasi-direct) band gap semiconductors. Note that although the most ubiquitous solar cell absorber, silicon, has an indirect band gap, a direct band gap, or at least a small difference between direct and indirect band gap, is beneficial for an efficient solar cell absorber.[45]

We conclude that, for photovoltaic applications, interesting candidates with direct band gaps are $CsSnCl_3$, $CsGeI_3$, $CsSnBr_3$, $RbGeBr_3$, $RbSnBr_3$, $BaPbO_3$, $CsSnI_3$, $InSnBr_3$, $RbGeI_3$, $RbSnCl_3$, $KGeBr_3$, $RbSnI_3$, $TlGeBr_3$, and $BaZrSe_3$ — most of them isovalent and closely related to $CsSnI_3$ and $CH_3NH_3PbI_3$, both of which have already been successfully utilized as light absorber and hole conductor in perovskite solar cells.[46] The only exceptions from this rule are $BaPbO_3$ and $BaZrSe_3$. As we show in Fig. ESI-2 in the ESI,† we find a rough correlation between larger band gaps of the compounds and larger electronegativity differences between the ions.

At this point, a comment about the importance of spin-orbit coupling (SOC) in these compounds is clearly in order. It should be remembered that the gaps shown here do not include the SOC correction, which is indeed very strong in the lead-based perovskites $CsPbI_3$ (SOC≈ 1.1 eV[47]; $E_g \approx 1.73$ eV[48]) and $MAPbI_3$ (SOC≈ 1 eV[49]; $E_g \approx$ 1.5–1-7 eV[42,50–53]), whereas in the tin-based perovskites it is reduced to about 0.2–0.45 eV.[54] Hence, neglecting SOC is not in all cases a mild approximation. However, although including SOC will decrease the gaps, we do not expect to obtain more interesting candidates with gaps in the right range for photovoltaics for the following reasons: looking at the list of band gaps, we see that the compounds with gaps between about 1.5 and 2 eV, which might in principle benefit from SOC, are either compounds where we expect small or moderate SOC, such as $CsSnCl_3$ or $BaSnO_3$, and/or they contain "unwanted" elements such as Tl or Tc.

In the region of band gaps smaller than 1 eV, we find several halides with In on the $B$ site instead of Pb or Sn, such as $CsInCl_3$ and $RbInBr_3$. Inspite of usually being a trivalent ion, In here plays the role of a divalent cation. It has been argued before, for example in Ref. 54, that in the lead and tin halides, the top of the valence band and the bottom of the conduction band are composed of orbitals located on the same atom, namely $s$ and $p$ orbitals of Pb or Sn, respectively, and that the high absorption coefficient of these compounds originates from the intraatomic transitions be-

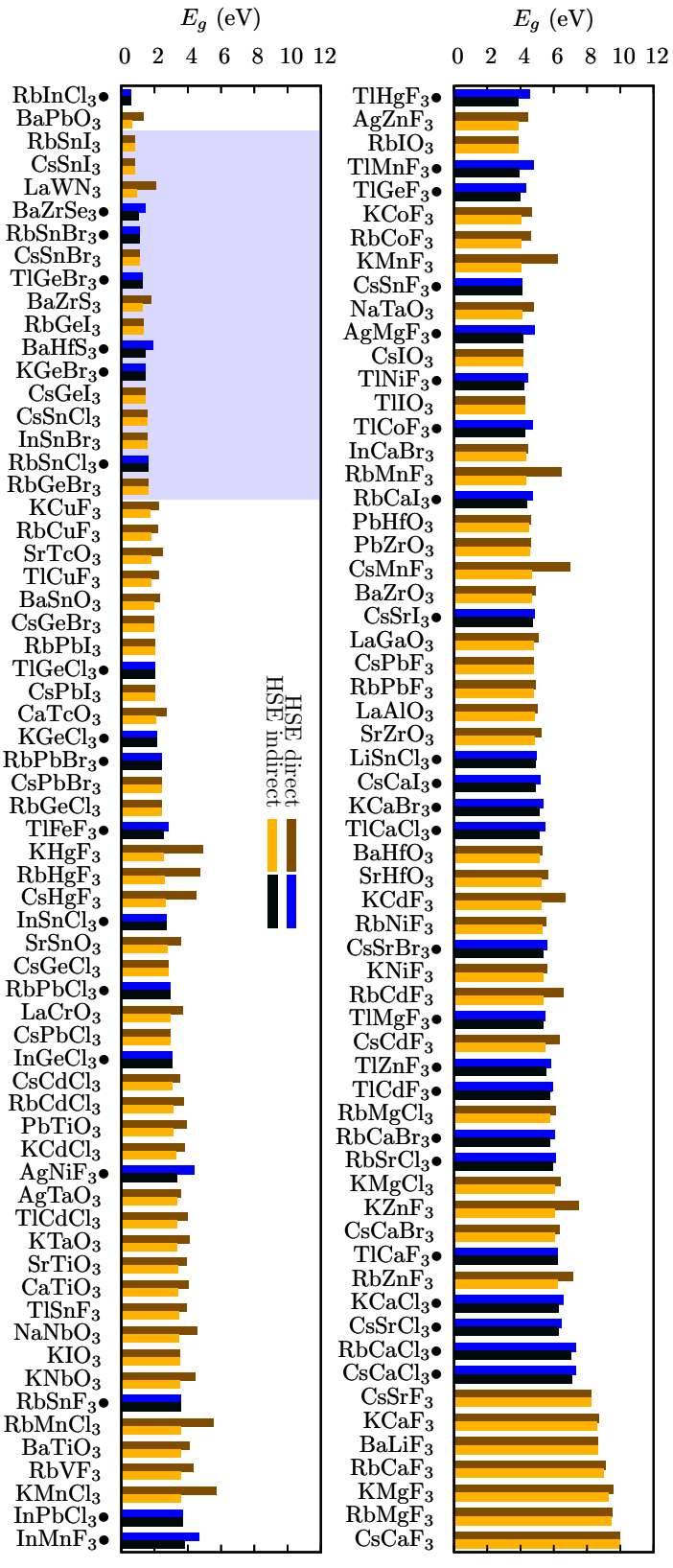


**Fig. 4** (Color online) Band gaps $E_g$ (where $E_g$ >0.5 eV) of the stable perovskites. New compounds are marked by a • and by the color blue.

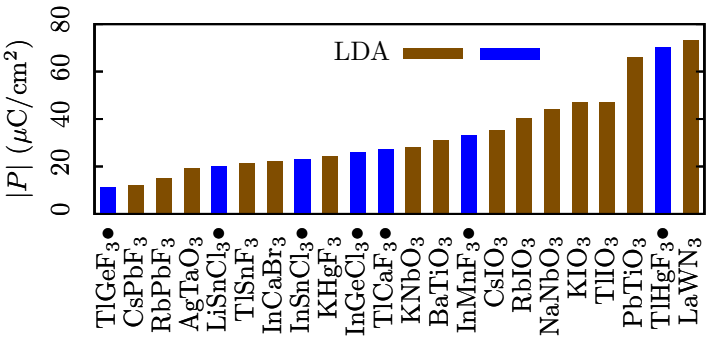


**Fig. 5** (Color online) Spontaneous electric polarization $|P|$ (where $|P| > 10$ $\mu$C/cm$^2$) of the stable perovskites. New compounds are marked by a • and by the color blue.

tween valence-band maximum and conduction-band minimum. This beneficial effect may hence always be possible in compositions where the lowest transitions are intraatomic and dipole-allowed. On the contrary, such strong absorption coefficients are not likely in perovskites where the participating atoms possess only a single valence state, such as in the case of Mg or Ca on *B* sites. In the case of In halides, we can expect that the valence band is composed partly of In *s* orbitals, and the conduction band of In *p* orbitals, so that the lowest optical transitions may occur between orbitals localized on the same site, just as in the lead and tin halides.[13,54] However, to make use of In halides, their band gap would need to be increased by alloying or possibly by exchanging the alkali atom by a larger organic molecule. Moreover, another drawback of In on *B* sites is that similar to Sn and Ge, it may lower the stability of the perovskite against oxidation.[13] We also find two compounds, $LaWN_3$, and $BaHfS_3$, that have suitable indirect band gaps and are not closely related to $CsPbI_3$, but their efficiency as light absorber will be limited by their large direct band gaps (larger than 1.9 eV for both compounds). It is however possible that the true ground states of these compounds differ from the ones determined here, and in that case their band gaps may move into the interesting range. As an example, in the case of $BaHfS_3$, we find indeed that the $NH_4CdCl_3$ prototype structure is more stable and has a lower direct band gap (1.69 eV instead of 1.93 eV), whereas the ground state of $LaWN_3$ (distorted perovskite with octahedral rotation) has a larger direct band gap of 2.23 eV.[41] Unfortunately, no other simple perovskite with a band-gap appropriate for photovoltaics seems to be sufficiently stable, apart from $BaPbO_3$ and $BaZrSe_3$. These results suggest that a possible solution to the stability of perovskite solar cells involves group V halides, whose properties may be further enhanced by alloying or related strategies, or possibly $BaPbO_3$, $BaZrSe_3$, and/or related compounds.

### 4.3 Ferroelectric polarization

In Fig. 5 we plot the spontaneous electric polarization of semiconducting perovskites with a polarization larger than 10 $\mu$C/cm$^2$. $PbTiO_3$ has one of the highest ferroelectric polarizations, and other well-known systems such as $KNbO_3$, $NaNbO_3$, and $BaTiO_3$ also appear at the top of the list.

**Table 3** Calculated ferroelectric polarization $|P|$, ferroelectric energy gain $E_{FE}$, indirect and direct band gap, and distance from the convex hull of stability $E_{hull}$ in eV/atom of $ABX_3$ perovskites with a ferroelectric polarization interesting for piezoelectrics. New compounds are marked by a •

| composition | $\|P\|$ ($\mu$C/cm$^2$) | $E_{FE}$ (eV/atom) | HSE gap ind. | HSE gap direct | $E_{hull}$ |
|---|---|---|---|---|---|
| $PbTiO_3$ | 66 | -0.010 | 3.15 | 3.95 | 0.000 |
| $BaTiO_3$ | 31 | -0.002 | 3.58 | 4.12 | 0.000 |
| $NaNbO_3$ | 44 | -0.008 | 3.50 | 4.55 | 0.000 |
| $CsPbF_3$ | 12 | -0.003 | 4.79 | 4.79 | 0.000 |
| $TlIO_3$ | 47 | -0.127 | 4.26 | 4.26 | 0.000 |
| $CsIO_3$ | 35 | -0.233 | 4.18 | 4.18 | 0.000 |
| $KNbO_3$ | 28 | -0.002 | 3.52 | 4.44 | 0.000 |
| $TlHgF_3$• | 70 | -0.070 | 3.86 | 4.57 | 0.000 |
| $RbIO_3$ | 40 | -0.143 | 3.88 | 3.88 | 0.001 |
| $InGeCl_3$• | 26 | -0.019 | 3.03 | 3.03 | 0.004 |
| $RbPbF_3$ | 15 | -0.029 | 4.80 | 4.91 | 0.007 |
| $KIO_3$ | 47 | -0.106 | 3.52 | 3.52 | 0.007 |
| $TlGeF_3$• | 11 | -0.072 | 3.99 | 4.33 | 0.007 |
| $InMnF_3$• | 33 | -0.003 | 3.81 | 4.65 | 0.011 |
| $KHgF_3$ | 24 | -0.015 | 2.55 | 4.91 | 0.016 |
| $InSnCl_3$• | 23 | -0.071 | 2.71 | 2.71 | 0.018 |
| $LiSnCl_3$• | 20 | -0.212 | 4.87 | 4.94 | 0.018 |
| $LaWN_3$ | 73 | -0.023 | 0.97 | 2.09 | 0.023 |
| $InCaBr_3$ | 22 | -0.052 | 4.32 | 4.47 | 0.028 |
| $TlCaF_3$• | 27 | -0.017 | 6.21 | 6.25 | 0.029 |
| $AgTaO_3$ | 19 | 0.000 | 3.38 | 3.61 | 0.039 |
| $TlSnF_3$ | 21 | -0.104 | 3.45 | 3.96 | 0.040 |

The corresponding values for the ferroelectric polarization are listed in Table 3, together with the energy gain with respect to the ideal cubic perovskite structure, the HSE band gap, and the distance to the convex hull.

When looking at the ferroelectric energy gain, we notice an enormous energy gain for $TlIO_3$, $CsIO_3$, $RbIO_3$, and $KIO_3$, much larger than for the other compounds, hinting that the ferroelectric Curie temperature could be very high in these unusual perovskite compounds.

We see that, remarkably, in our list of almost 200 stable $ABX_3$ perovskites, there are not much more than 20 compounds for which a ferroelectric distortion is stable. Instead, in all other stable ferroelectric perovskites, any ferroelectric distortion must be accompanied and stabilized by other modes, such as octahedral rotations.

An unusual perovskite, though not suitable as absorber in single-junction solar cells due to its large band gap, is the nitride perovskite $LaWN_3$. We studied nitride perovskites in a recent publication using *ab initio* structural prediction.[41] $LaWN_3$ exhibits a band gap potentially interesting for multilayer solar cell absorbers, and it has a large ferroelectric polarization, which makes it a possible candidate for piezoelectric applications. Here we find a slightly smaller band gap and larger ferroelectric polarization than that in Ref. 41, as the crystal structure is not the same. In fact, the octahedral rotation which is present in the ground state structure of Ref. 41 decreases the energy by 23 meV/atom and reduces the ferroelectric polarization by 7 $\mu$C/cm$^2$. We remind that this rotational distorsion of the octahedra network is missing here, since it requires a unit cell with at least 10 atoms. Our distance from the convex hull of $LaWN_3$ is measured with respect to the ground state of Ref. 41.

All the perovskites in our list with a suitable band gap for photovoltaic absorbers have, within an estimated error bar of about 5 $\mu$C/cm$^2$, vanishing or very small ferroelectric polarizations.

Within the inorganic perovskites with 5-atom unit cells, it is apparently impossible to have a compound with a bandgap suitable for photovoltaics, and at the same time a sizeable ferroelectric polarization. Hence, if one requests internal electric fields arising from ferroelectricity or local dipole moments in order to decrease recombination, one must either continue to work with a molecule with a dipole moment on the *A* site, such as MA, or alloy with a ferroelectric.

A ferroelectric polarization is not a necessary requirement for an absorber material, but it is assumed to help separating the photogenerated charges, due to the buildup of local electric fields.[55] Although there is now evidence that $MAPbI_3$ is not (strongly) ferroelectric at room temperature,[56] still there may be small fluctuating polarization domains which could create local electric fields. Besides, ferroelectric or other lattice instabilities, if energetically close to the ground state, will enhance phononic screening of excitons and help increasing the carrier life time. In any case, a ferroelectric polarization, or at least a lattice instability that favors local dipole moments, is likely a plus.

### 4.4 Effective masses

In Fig. 6, we show the effective hole masses. The lowest hole masses are obtained for (Cs,Rb)(Ge,Sn,Pb)$F_3$, which points to the ability of these compounds to exhibit fast hole transport and low carrier recombination rates.

**Table 4** Calculated HSE band gaps, effective hole mass $m_h^*$, and distance from the convex hull of stability $E_{hull}$ in eV/atom of $ABX_3$ perovskites with gaps and effective masses potentially interesting for TCO's. New compounds are marked by a •

| composition | HSE gap ind. | HSE gap direct | $m_h^*$ | $E_{hull}$ |
|---|---|---|---|---|
| $PbTiO_3$ | 3.15 | 3.95 | 0.69 | 0.000 |
| $CsPbF_3$ | 4.79 | 4.79 | 0.41 | 0.000 |
| $CsSnF_3$• | 4.10 | 4.10 | 0.60 | 0.003 |
| $InGeCl_3$• | 3.03 | 3.03 | 0.53 | 0.004 |
| $RbPbF_3$ | 4.80 | 4.91 | 0.39 | 0.007 |
| $KIO_3$ | 3.52 | 3.52 | 0.97 | 0.007 |
| $KMnCl_3$ | 3.62 | 5.73 | 0.67 | 0.010 |
| $InPbCl_3$• | 3.69 | 3.71 | 0.86 | 0.019 |
| $RbMnCl_3$ | 3.58 | 5.56 | 0.67 | 0.021 |
| $RbCdCl_3$ | 3.12 | 3.74 | 0.98 | 0.025 |
| $KCdCl_3$ | 3.31 | 3.82 | 0.92 | 0.038 |
| $TlCdCl_3$ | 3.38 | 3.99 | 0.87 | 0.050 |
| $RbSnF_3$• | 3.57 | 3.58 | 0.32 | 0.052 |

In Table 4 we list all candidates with band gaps in a range interesting for *p*-type transparent conductors and their hole effective masses. We find several materials that fullfill both conditions of transparency (band gap larger than 3 eV) and small hole effective mass: $PbTiO_3$, $CsPbF_3$, $CsSnF_3$, $InGeCl_3$, $RbPbF_3$, $KIO_3$, $KMnCl_3$, $InPbCl_3$, $RbMnCl_3$, $RbCdCl_3$, $KCdCl_3$, $TlCdCl_3$, and $RbSnF_3$. These compounds are hence possible candidates for the long-missing *p*-type transparent conductors, although further theoretical characterization including defects and strategies for *p*-doping is still required.

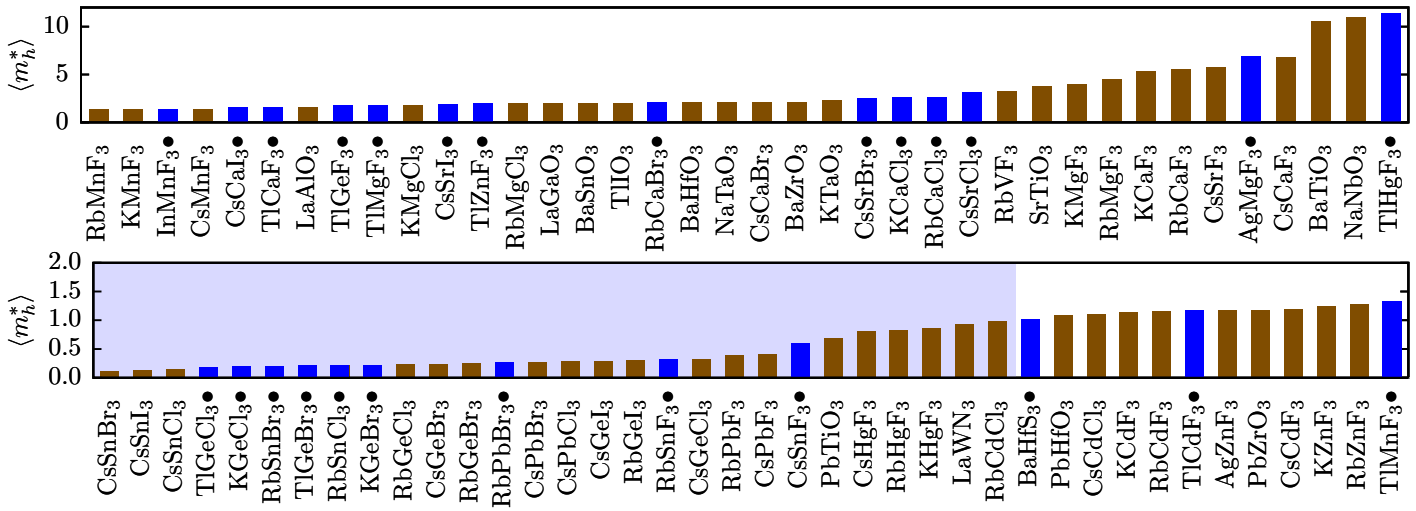


**Fig. 6** (Color online) Effective hole masses in units of the electron mass, direction-averaged. Hole masses $\leq 1$ are shaded in blue. New compounds are marked by a • and by the color blue.

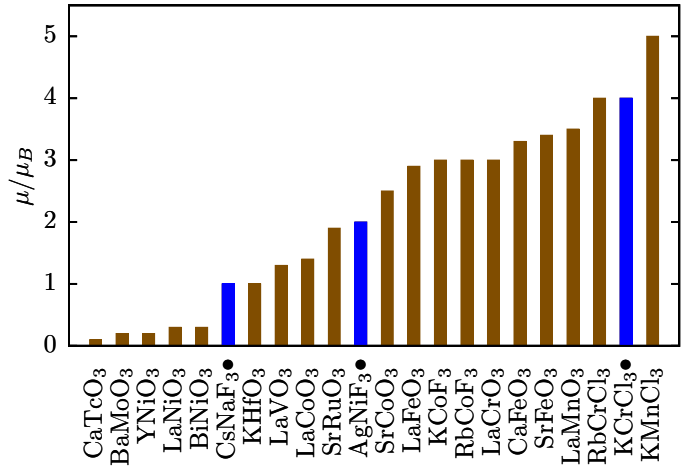


**Fig. 7** (Color online) Total magnetic moments per 5-atom unit cell. New compounds are marked by a • and by the color blue.

As we show in the ESI† in Fig. ESI-3, we find a general trend of increase of the effective hole mass with increasing band gap for direct-bandgap semiconductors.

### 4.5 Magnetic moments

Finally, we show in Fig. 7 the total magnetic moments per 5-atom unit cell of the magnetic perovskite compounds. It is not a great surprise that the largest magnetic moments are obtained with Mn, Fe, Co, Cr, and to a smaller extent with V, Ni, or Ru on the *B* site. The highest magnetic moments of about 4–5 $\mu_B$ are obtained with Mn or Cr on the *B* site, namely in $RbCrCl_3$, $KCrCl_3$, and $KMnCl_3$. Whereas some of these compounds are listed, for example, in the Materials Project database, others are not yet explored, such as $KCrCl_3$, $AgNiF_3$, and $CsNaF_3$, or $InMnF_3$. Antiferromagnetic $InMnF_3$ is particularly interesting as a multiferroic semiconductor with a sizeable ferroelectric polarization of 33 $\mu C/cm^2$ and simultaneously a large antiferromagnetic moment of $\approx 5$ $\mu_B$ per 5-atom unit cell, which makes it a promising candidate for piezoelectric and/or magnetoelectric applications.

In total we find 25 compounds with Cu, Ag, or Au on the octahedral *B* site, with a formal ionic charge of 2+ and a half-filled *d* orbital. These compounds are expected to undergo a Jahn-Teller distortion of the octahedral geometry, providing an energetic stabilization by removing the electronic degeneracy of the highest occupied molecular orbitals. This distortion can have strong effects on the magnetic properties of the compound, as in the case of $KAgF_3$ [57,58]. For $KAgF_3$, PBE calculations fail to yield the correct antiferromagnetic ground-state structure. Although our approach allows for the Jahn-Teller effect, a correct description of the true ground state of these materials would require to take into account crystal structures beyond our list of prototypes, in combination with a higher level of theory, such as DFT+*U* or possibly a hybrid functional.

## 5 Summary and Conclusion

In this work we have explored the whole periodic table searching for inorganic perovskites. Thanks to high-throughput density functional theory calculations, we obtained a "catalogue" of potentially thermodynamically stable perovskites in the cubic structure or in slightly distorted variants and we have characterized their electronic properties. Starting from over 32000 possible $ABX_3$ compounds, we found 199 stable perovskites (within 25 meV from the convex hull). We note that 71 compounds are new, as they are absent from databases of known materials. For this set of 199 perovskites we have calculated band gaps, ferroelectric polarization, effective hole masses, and magnetic moments. These properties are relevant for photovoltaic, piezoelectric, and magnetic applications.

Concerning photovoltaics, among the stable perovskite compounds, the only systems with a suitable electronic band gap, besides $BaPbO_3$ and $BaZrSe_3$, are alkali lead, tin, and germanium halide perovskites. At the same time, those are also the compositions with the lowest effective hole masses. This suggests that the most promising strategy to improve the stability of the per-

ovskite absorbers is alloying and/or doping of one or several of the inorganic group IV halides, or to explore compounds related to $BaPbO_3$ and $BaZrSe_3$.

Concerning piezoelectric applications, we find a few new ferroelectric perovskites: $LaWN_3$, $TlHgF_3$, $InGeCl_3$, $TlGeF_3$, $INMnF_3$, $InSnCl_3$, $LiSnCl_3$, and $TlCaF_3$, the most interesting novel candidate being $LaWN_3$ (large ferroelectric polarization similar to that of $PbTiO_3$). We find that compounds with iodine on the *B* site, such as $RbIO_3$, $CsIO_3$, $KIO_3$, and $TlIO_3$, have very large energy difference between paraelectric and ferroelectric phase, which hints at a high ferroelectric Curie temperature.

About ten perovskites, most of them halides, have band gaps large enough to be transparent and at the same time have small hole effective masses. These compounds should be further studied as promising candidates for *p*-type transparent conductors.

Finally, we find several manganese and chromium halides with remarkably large magnetic or antiferromagnetic moments ($> 4\mu_B$ per formula unit). Two of them are not contained in databases: $KCrCl_3$, and $InMnF_3$. For one of them, $InMnF_3$, we find simultaneously a large ferroelectric polarization of 33 $\mu C/cm^2$ and a large antiferromagnetic moment of $\approx 5\ \mu_B$ per 5-atom unit cell.

Our calculations reinforce the idea that perovskites are a family of materials with extraordinary properties that deserve to be further explored.

## 6 Acknowledgement

We acknowledge inspiring and instructive discussions that took place during the workshop "Perovskite solar cells: the quest for a theoretical description", organized by the Centre Européen de Calcul Atomique et Moléculaire (CECAM) in August 2015. We acknowledge support from the French ANR (ANR-12-BS04-0001-02). Computational resources were provided by the Leibniz Supercomputing Centre (SuperMUC, project number pr84ra). Crystal structures were visualized with VESTA,[59] gnuplot and python-matplotlib were used for the other graphs. Shannon radii were retrieved from the Database of Ionic Radii of the Atomistic Simulation Group at Imperial College London[60].

## References

1 B. Jaffe, *Piezoelectric ceramics*, Elsevier, 2012, vol. 3.
2 M. E. Lines and A. M. Glass, *Principles and applications of ferroelectrics and related materials*, Oxford University Press, 1977.
3 A. Kojima, K. Teshima, Y. Shirai and T. Miyasaka, *J. Am. Chem. Soc.*, 2009, **131**, 6050–6051.
4 J. Wang, J. B. Neaton, H. Zheng, V. Nagarajan, S. B. Ogale, B. Liu, D. Viehland, V. Vaithyanathan, D. G. Schlom, U. V. Waghmare, N. A. Spaldin, K. M. Rabe, M. Wuttig and R. Ramesh, *Science*, 2003, **299**, 1719–1722.
5 S. Aharon, A. Dymshits, A. Rotem and L. Etgar, *J. Mat. Chem. A*, 2015, **3**, 9171–9178.
6 S. D. Stranks and H. J. Snaith, *Nature nanotechnology*, 2015, **10**, 391–402.
7 http://en.wikipedia.org/wiki/Solar_cell.
8 G. Giorgi, J.-I. Fujisawa, H. Segawa and K. Yamashita, *J. Phys. Chem. Lett.*, 2013, **4**, 4213–4216.
9 W.-J. Yin, J.-H. Yang, J. Kang, Y. Yan and S.-H. Wei, *J. Mat. Chem. A*, 2015, **3**, 8926–8942.
10 G. Niu, X. Guo and L. Wang, *J. Mater. Chem. A*, 2015, **3**, 8970–8980.
11 Y.-Y. Zhang, S. Chen, P. Xu, H. Xiang, X.-G. Gong, A. Walsh and S.-H. Wei, *AIP Adv.*, 2015, 01301.
12 K. P. Marshall, R. I. Walton and R. A. Hatton, *J. Mat. Chem. A*, 2015, **3**, 11631–11640.
13 G. Giorgi and K. Yamashita, *Chem. Lett.*, 2015, **44**, 826–828.
14 Y.-Y. Sun, M. L. Agiorgousis, P. Zhang and S. Zhang, *Nano Lett.*, 2015, **15**, 581–585.
15 G. Ceder, *Materials Research Bulletin*, 2010, **35**, 693–701.
16 X. Zhang, Y. Wang, J. Lv, C. Zhu, Q. Li, M. Zhang, Q. Li and Y. Ma, *J. Chem. Phys.*, 2013, **138**, 114101.
17 H. Katayama-Yoshida, K. Sato, H. Kizaki, H. Funashima, I. Hamada, T. Fukushima, V. Dinh and M. Toyoda, *Appl. Phys. A*, 2007, **89**, 19–27.
18 G. Hautier, A. Miglio, G. Ceder, G.-M. Rignanese and X. Gonze, *Nature communications*, 2013, **4**, 2292.
19 V. Sharma, C. Wang, R. G. Lorenzini, R. Ma, Q. Zhu, D. W. Sinkovits, G. Pilania, A. R. Oganov, S. Kumar, G. A. Sotzing *et al.*, *Nature communications*, 2014, **5**, 4845.
20 N. Drebov, A. Martinez-Limia, L. Kunz, A. Gola, T. Shigematsu, T. Eckl, P. Gumbsch and C. Elsässer, *New J. Phys.*, 2013, **15**, 125023.
21 R. Caracas and R. E. Cohen, *Appl. Phys. Lett.*, 2007, **91**, 092902.
22 R. Armiento, B. Kozinsky, M. Fornari and G. Ceder, *Phys. Rev. B*, 2011, **84**, 014103.
23 I. E. Castelli, T. Olsen, S. Datta, D. D. Landis, S. Dahl, K. S. Thygesen and K. W. Jacobsen, *Energy Environ. Sci.*, 2012, **5**, 5814–5819.
24 I. E. Castelli, D. D. Landis, K. S. Thygesen, S. Dahl, I. Chorkendorff, T. F. Jaramillo and K. W. Jacobsen, *Energy Environ. Sci.*, 2012, **5**, 9034–9043.
25 M. R. Filip, G. E. Eperon, H. J. Snaith and F. Giustino, *Nature communications*, 2014, **5**, 5757.
26 J. A. Brehm, J. W. Bennett, M. R. Schoenberg, I. Grinberg and A. M. Rappe, *J. Chem. Phys.*, 2014, **140**, 224703.
27 http://en.wikipedia.org/wiki/Electronegativity, 2015.
28 A. Jain, S. P. Ong, G. Hautier, W. Chen, W. D. Richards, S. Dacek, S. Cholia, D. Gunter, D. Skinner, G. Ceder and K. A. Persson, *APL Materials*, 2013, **1**, 011002.
29 J. E. Saal, S. Kirklin, M. Aykol, B. Meredig and C. Wolverton, *JOM*, 2013, **65**, 1501–1509.
30 V. M. Goldschmidt, *Naturwissenschaften*, 1926, **14**, 477–485.
31 R. T. Shannon, *Acta Cryst. A*, 1976, **32**, 751–767.
32 A. Akimov, G. Savchuk, V. Rubtsov and A. Letko, *Crystallography Reports*, 2003, **48**, 239–243.
33 J. P. Perdew, K. Burke and M. Ernzerhof, *Phys. Rev. Lett.*, 1996, **77**, 3865–3868.

34 G. Kresse and J. Furthmüller, *Comput. Mater. Sci.*, 1996, **6**, 15–50.

35 C. B. Barber, D. P. Dobkin and H. Huhdanpaa, *ACM Transactions on Mathematical Software (TOMS)*, 1996, **22**, 469–483.

36 J. Heyd, G. E. Scuseria and M. Ernzerhof, *J. Chem. Phys.*, 2003, **118**, 8207–8215.

37 G. K. Madsen and D. J. Singh, *Comput. Phys. Commun.*, 2006, **175**, 67–71.

38 M. Gajdos, K. Hummer, G. Kresse, J. Furthmüller and F. Bechstedt, *Phys. Rev. B*, 2006, **73**, 045112.

39 L. Sun, Y.-F. Chen, W.-H. Ma, L.-W. Wang, T. Yu, M.-S. Zhang and N.-B. Ming, *Applied physics letters*, 1996, **68**, 3728–3730.

40 H. Glawe, A. Sanna, E. K. U. Gross and M. A. L. Marques, *New J. Phys.*, 2015, submitted.

41 R. Sarmiento-Perez, T. F. T. Cerqueira, S. Körbel, S. Botti and M. A. L. Marques, *Chem. Mater.*, 2015, **27**, 5957–5963.

42 C. C. Stoumpos, C. D. Malliakas and M. G. Kanatzidis, *Inorg. Chem.*, 2013, **52**, 9019–9038.

43 D. J. Singh, Q. Xu and K. P. Ong, *Appl. Phys. Lett.*, 2014, **104**, 011910.

44 W. Zhang, J. Tang and J. Ye, *J. Mater. Res.*, 2007, **22**, 1859–1871.

45 L. Yu and A. Zunger, *Phys. Rev. Lett.*, 2012, **108**, 068701.

46 I. Chung, B. Lee, J. He, R. P. Chang and M. G. Kanatzidis, *Nature*, 2012, **485**, 486–489.

47 J. Even, L. Pedesseau, J.-M. Jancu and C. Katan, *J. Phys. Chem. Lett.*, 2013, **4**, 2999–3005.

48 G. E. Eperon, S. D. Stranks, C. Menelaou, M. B. Johnston, L. M. Herz and H. J. Snaith, *Energy Environ. Sci.*, 2014, **7**, 982–988.

49 F. Brivio, K. T. Butler, A. Walsh and M. van Schilfgaarde, *Phys. Rev. B*, 2014, **89**, 155204.

50 H.-S. Kim, C.-R. Lee, J.-H. Im, K.-B. Lee, T. Moehl, A. Marchioro, S.-J. Moon, R. Humphry-Baker, J.-H. Yum, J. E. Moser *et al.*, *Scientific Reports*, 2012, **2**, 591.

51 T. Baikie, Y. Fang, J. M. Kadro, M. Schreyer, F. Wei, S. G. Mhaisalkar, M. Graetzel and T. J. White, *J. Mat. Chem. A*, 2013, **1**, 5628–5641.

52 Y. Yamada, T. Nakamura, M. Endo, A. Wakamiya and Y. Kanemitsu, *Appl. Phys. Express*, 2014, **7**, 032302.

53 T. Ishihara, *Journal of Luminescence*, 1994, **60**, 269–274.

54 L.-y. Huang and W. R. L. Lambrecht, *Phys. Rev. B*, 2013, **88**, 165203.

55 J. M. Frost, K. T. Butler, F. Brivio, C. H. Hendon, M. van Schilfgaarde and A. Walsh, *Nano Lett.*, 2014, **14**, 2584–2590.

56 A. Stroppa, C. Quarti, F. D. Angelis and S. Picozzi, *J. Phys. Chem. Lett.*, 2015, **6**, 2223–2231.

57 D. Kurzydłowski, Z. Mazej, Z. Jagličić, Y. Filinchuk and W. Grochala, *Chem. Commun.*, 2013, **49**, 6262–6264.

58 Z. Mazej, E. Goreshnik, Z. Jagličić, B. Gaweł, W. Łasocha, D. Grzybowska, T. Jaroń, D. Kurzydłowski, P. Malinowski, W. Koźminski *et al.*, *CrystEngComm*, 2009, **11**, 1702–1710.

59 K. Momma and F. Izumi, *J. Appl. Crystallogr.*, 2011, **44**, 1272–1276.

60 `http://abulafia.mt.ic.ac.uk/shannon`, 2015.